Title
Dynamics of Surface Alloys: Rearrangement of Pd/Ag(111) Induced by CO and O2

Journal
The Journal of Physical Chemistry C, 123(13)

ISSN
1932-7447

Authors
van Spronsen, Matthijs A
Daunmu, Kaining
O'Connor, Christopher R
et al.

Publication Date
2019-04-04

DOI
10.1021/acs.jpcc.8b08849

Peer reviewed

Dynamics of Surface Alloys: Rearrangement of Pd/Ag(111) Induced by CO and O_2

Matthijs A. van Spronsen,[†,‡,◆] Kaining Daunmu,[§,◆] Christopher R. O'Connor,[†] Tobias Egle,[†,∥] Heath Kersell,[‡] Judit Oliver-Meseguer,[⊥] Miquel B. Salmeron,[‡,⊥,#] Robert J. Madix,[∥] Philippe Sautet,[§,▽] and Cynthia M. Friend[*,†,∥]

[†]Department of Chemistry and Chemical Biology, Harvard University, Cambridge, Massachusetts 02138, United States
[‡]Materials Sciences Division, Lawrence Berkeley National Laboratory, Berkeley, California 94720, United States
[§]Department of Chemical and Biomolecular Engineering, University of California, Los Angeles, California 90095, United States
[∥]School of Engineering and Applied Sciences, Harvard University, Cambridge, Massachusetts 02138, United States
[⊥]Chemical Science Division, Lawrence Berkeley National Laboratory, Berkeley, California 94720, United States
[#]Department of Materials Science and Engineering, University of California, Berkeley, California 94720, United States
[▽]Department of Chemistry and Biochemistry, University of California, Los Angeles, California 90095, United States

ABSTRACT: Alloys of Ag and small amounts of Pd are promising as bifunctional catalysts, potentially combining the inherent selectivity of the noble Ag with that of the more reactive Pd. Stable PdAg surface alloys are prepared via evaporation of Pd onto Ag(111) at room temperature followed by annealing at 400 K to create a model system. Using this procedure, the most stable form of the surface alloy under vacuum was determined to be a Ag-capped PdAg surface alloy, on the basis of a combination of X-ray photoelectron spectroscopy (XPS), scanning tunneling microscopy (STM), and density functional theory (DFT). Extensive roughening of the surface was apparent in STM images, characterized by islands of the Ag/PdAg/Ag(111) alloy of several layers thickness. The roughening is attributed to transport of Ag from the Ag(111) surface into the alloy islands. Within these islands, there is a driving force for Pd to be dispersed, surrounded by Ag, on the basis of DFT modeling. Exposure of these Ag/PdAg/Ag(111) islands to CO (0.5 Torr) at 300 K induces migration of Pd to the surface, driven by the energetic stabilization of the Pd−CO bond based on ambient-pressure XPS. Once the Pd is drawn to the surface by higher pressures of CO at room temperature, it remains stable even under very low CO partial pressures at temperatures of 300 K and below, on the basis of DFT-modeled phase behavior. Exposure to 1 Torr of O_2 at 400 K also causes Pd to resurface, and the resulting structure persists even at low pressures and temperatures below 300 K. These results establish that the state of the PdAg catalyst surface depends strongly on pretreatment and operational conditions. Hence, exposure of an alloy catalyst to CO or O_2 at moderate temperatures and pressures can lead to catalyst activation by bringing Pd to the surface. Furthermore, these results demonstrate that exposure to CO at room temperature, which is often used as a proxy for evaluating the Pd coordination sites available in a catalyst, changes the surface structure. Therefore, the CO vibrational frequencies measured with diffuse-reflectance infrared Fourier-transform spectroscopy (DRIFTS) on PdAg catalyst materials do not necessarily provide information about their working state, and fundamental understanding of the CO-PdAg alloy is crucial.

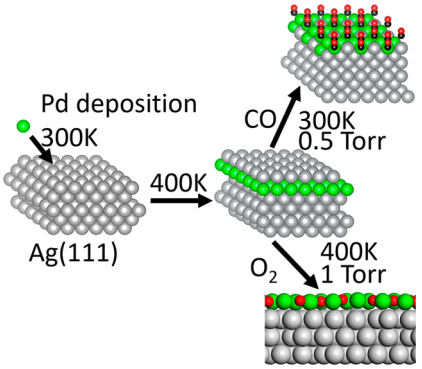

INTRODUCTION

Metal alloys are widely studied in heterogeneous catalysis because of their potential for emergent properties (properties distinct from the individual components). Specifically, alloys have the potential to increase reaction selectivity beyond each single component, thereby increasing the efficiency of catalytic processes and decreasing energy usage for chemical synthesis. Distinct properties can arise in alloys because of changes in electronic structure. Such changes, which depend on the structure and composition of the material, will dictate the chemical properties of alloys. In heterogeneous catalysis, the bonding environment at the surface is particularly important, because the surface directly interacts with reactants and products.

The optimal design of alloy catalysts is governed by the composition, configuration, and structure of the material to

achieve high reactivity and selectivity. However, tailoring the surface concentration and distribution of the different metals in an alloy is a significant challenge because both kinetic and thermodynamic factors can play a vital role. Thermodynamically, the interaction of the gas phase with the surface can strongly affect the surface free energy. For example, the presence of H_2 induces the enrichment of Pt at the surface of $Pt_{50}Co_{50}$ nanoparticles.[1,2] Conversely, Co segregation and formation of CoO occurred under oxidizing conditions.[2] Similarly, compositional changes have been observed for RhPd,[3] PtPd,[3] and PtSn[4] nanoparticles and single-crystal alloys, such as NiPt/Pt(111) and CoPt/Pt(111).[5] In addition, metastable, kinetically trapped structures may also be formed and maintained during catalysis as is for the surface of a nanoporous $Ag_{0.03}Au_{0.97}$ alloy enriched in Ag by activation in an oxidizing environment; the surface remains enriched in Ag under net reducing reaction conditions in alcohol coupling because of the relatively low temperature used in the process.[6]

Herein, we focused on the behavior of a surface alloy of Pd on Ag(111). Alloys that contain Ag are of particular interest because they are capable of catalyzing highly selective reactions as a consequence of the relatively weak binding of reaction intermediates to these surfaces and the associated low activity for bond scission in key intermediates. Palladium was investigated primarily because PdAg alloys are used as a means of increasing reaction selectivity for partial hydrogenation of alkynes[7−11] and acrolein.[12]

The low inherent reactivity of Ag is illustrated by the absence of reaction of most molecules on its atomically clean surfaces. For example, alkenes,[13−17] alkynes,[18,19] aldehydes,[20,21] and alcohols[22−24] all reversibly desorb from well-prepared low Miller index surfaces of Ag. Furthermore, H_2 does not dissociate on Ag, and atomic H is only very weakly bound, desorbing below room temperature.[25−27]

The potential for highly selective reactions on the relatively inert Ag is illustrated by coadsorption of H and reactant molecules with C═C and C═O bonds on Ag(111). Consistent with the single-crystal studies, hydrogenation of the C═O bond of acrolein is also observed on a supported Ag catalyst, albeit with low activity.[28] The presence of adsorbed H on Ag(111), created by exposure of H atoms to the surface, leads to hydrogenation of the C═O bonds in acrolein[29] and crotonaldehyde.[30] The ability to hydrogenate the C═O bond on Ag(111) is attributed to tilting of the C═C bond away from the surface induced by the adsorbed H.[29] More recently, the selectivity for hydrogenation of C═O vs C═C bonds in α,β-unsaturated carbonyl compounds, acrolein and isophorone, on Cu, Ag, and Au was related to the degree of interaction of higher energy molecular orbitals. Strong interaction of the C═C bond of acrolein even with Ag(111) leads to substantial inner-orbital broadening and C═C activation, similar to Pd. In contrast, the C═C bond of isophorone is not significantly broadened, leading to preferential C═O bond hydrogenation.[31]

An array of selective oxidation reactions can also be induced on Ag when O(ads) is present.[32] The challenge is to create key reactive intermediates, such as H(ads) and O(ads), that can initiate the catalytic cycle on the Ag in order to have high activity with high selectivity.

Creation of Ag alloys has the potential of achieving the goal of initiating surface reactions on the Ag while retaining high selectivity. The concept is to create Ag-based alloys containing a more reactive metal, such as Pd. However, for the Pd to affect reactivity, it must be on or near the surface. Furthermore, the distribution of Pd on the surface will affect selectivity. Large islands of Pd are expected to lead to lower reaction selectivity as they approach behavior similar to the bulk. Even though PdAg nanoparticle alloys have been tested for selective hydrogenation, their structure and composition under reaction conditions is generally not well understood.[33]

The requirement of Pd to be on the surface to affect reactivity is complicated by the fact that Ag has a substantially lower surface free energy than Pd.[34] Accordingly, the surface of PdAg alloys is expected to be highly enriched in Ag for a clean surface.[35−37] On the other hand, reactant gases can be used to induce segregation of Pd on the surface if they are more strongly bonded to Pd than Ag and if the thermal energy is sufficient for mobility of the Pd in Ag. A combination of experimental and theoretical approaches was used to understand the behavior of PdAg surface alloys, including in the presence of reactive gases. DFT-based Monte Carlo simulations have recently shown a strong segregation of Pd to the surface when the PdAg alloy is subjected to a pressure of acetylene.[38,39]

In this work, a PdAg surface alloy was created by deposition of small amounts of Pd on the Ag(111) surface and used as a model for the behavior of PdAg alloy catalysts. As anticipated, Pd at the surface was not favored in vacuum, but instead of migrating to the subsurface region, the Pd became covered by a capping layer of Ag, generating a surface that is essentially pure Ag after deposition and heating to 400 K. The strong effect of reactant gases on the alloy structure and composition is illustrated by the resurfacing of the Pd upon exposure of the Ag-terminated surface to CO or O_2 at ambient pressure, even at room temperature. These results demonstrate the high mobility of Pd in a PdAg surface alloy even at moderate temperatures and have implications for understanding catalyst activation and analysis. Specifically, the vibrational frequency of CO is often used to draw conclusions about the types of Pd sites available during reaction; however, our work shows that the CO will fundamentally change the structure of the alloy. Second, the fact that oxygen draws Pd to the surface indicates that the typical catalyst pretreatment by calcination (heating in O_2) will also change the composition of the material.

In the spirit of honoring Professors Freund and Sauer, we demonstrate here the power of combining experimental and theoretical approaches to understand the importance of bonding and reactivity in heterogeneous catalysis. Through their leadership and their established collaboration, Freund and Sauer have made intellectual breakthroughs and have advanced methodology to advance the field. We are grateful for their many contributions.

MATERIALS AND METHODS

Sample Preparation. The surface alloys were formed using Ag single crystals (Table S1) as substrate with a surface polished to the (111) plane. The Ag(111) crystals were cleaned by Ar^+ sputtering (1 keV) followed by annealing to 770−800 K in ultrahigh vacuum (UHV). The polished crystals were treated with 20−30 of these cycles before conducting any experiment. After transfer through air, around 10 cleaning cycles were completed before starting measurements. Between experiments, the samples were cleaned with 2−3 cycles with the last cycle using Ar^+ accelerated at 0.5 kV and a milder anneal, typically 25 K lower in temperature. After cleaning the surface, the structure was inspected with scanning tunneling

microscopy (STM), showing regions with predominantly extended terraces separated by regions with higher step density. The presence of extended (111) terraces was confirmed by the sharp low-energy electron diffraction (LEED) pattern (Figure S1, Section S2). Carbon was persistently measured with X-ray photoelectron spectroscopy (XPS) on the crystal from the surface preparation laboratory (SPL) and was, therefore, extensively cleaned with 2 keV Ar^+, followed by a flash anneal to 800 K in UHV (94 cycles). The absence of impurities was determined (Figure S2, Section S2) with ion scattering spectroscopy (ISS), using 1.5−2.0 keV $^4He^+$, Auger electron spectroscopy (AES) (Figure S3, Section S2), and XPS measurements.

Palladium was evaporated onto clean Ag(111) from a rod with a purity of 99.99% using electron-beam evaporators and deposited at room temperature at a rate of $(2-3) \times 10^{-3}$ ML/s. The evaporators were water cooled to minimize outgassing and thoroughly degassed prior each use. The amount of deposited Pd was estimated *directly after deposition, i.e., prior to any annealing*. The coverage was estimated based on the Pd/Ag ratio measured by AES (before the STM measurements) or by XPS. The measured areas (XPS) or peak intensities (AES) were corrected for element specific and experimental factors as described in the Supporting Information (Tables S2 and S3, Section S3). The Pd coverage estimate assumed that all Pd remained on the surface at the deposition temperature of 300 K. This calculation underestimates the amount of deposited Pd if Pd does not remain on the surface. The estimated coverage was used to calculate the deposition rate. After deposition, the Pd was annealed for several minutes to 400−452 K in UHV.

Gas lines were baked under vacuum and flushed several times before dosing gases. Gas doses are reported in Langmuir, defined as 1×10^{-6} Torr × s. For sputtering, high-purity Ar was used [Matheson, 99.9999% (UHV XPS) Praxair Ultra High Purity, 99.999% (AP XPS), and Airgas, 99.999% (STM)]. To oxidize Pd/Ag(111), high-purity O_2 (Praxair 5.0 research) was used. For CO, a mixture (Airgas) of 20% CO (purity of 99.9%) in Ar (UHV XPS) and pure CO (Praxair; purity of 99.99%) was used.

X-ray Photoelectron Spectroscopy (UHV). The UHV XPS system consisted of an analysis chamber (base pressure $\sim 1 \times 10^{-10}$ Torr) and a preparation chamber [base pressure $(2-3) \times 10^{-10}$ Torr], housing an electron-beam evaporator (Focus EFM3) and a sputter gun (Perkin Elmer 04-161). The UHV XPS measurements employed an X-ray source (Perkin Elmer 04-548/32-095 with RBD 20-042) using (nonmonochromatized) Mg Kα radiation. The sample was irradiated under an angle of 43°, and the photoelectrons were measured with normal emission using a hemispherical analyzer (SPECS Phoibos 100 equipped with a 5-channel electron multiplier), at a pass energy of 10 eV and the lenses set to large-area mode. The binding energy was calibrated by setting the Ag $3d_{5/2}$ peak to 368.2 eV.[40] Referencing the binding energy to the Fermi level was not possible due to the overlap with the Ag 4d band excited by Mg Kα_3.[41] The analysis chamber further housed LEED optics (PHI 15-120) and quadrupole mass spectrometry (QMS; Hiden RGA) equipment. The sample was in thermal contact with N_2(l), cooling the sample to ∼85 K, and could be heated by thermal radiation from a thoriated tungsten filament located behind the sample. The temperature was measured with a K-type thermocouple placed in a hole in the center of the sample.

X-ray Photoelectron Spectroscopy (AP). The ambient-pressure (AP) XPS experiments were performed at the bending-magnet beamline 9.3.2 of the Advanced Light Source at the Lawrence Berkeley National Laboratory. Additional experimental details are included in the Supporting Information (Section S1).

For the 3d regions of Ag and Pd, both spin−orbit-splitting components were measured, but only the $3d_{5/2}$ regions are shown. The spectra were plotted after subtraction of a linear background fitted to the low binding-energy side of the spectra to account for a globally varying background. Subsequently, a Shirley background describing the local inelastic background was subtracted. Selected spectra were fitted to study the contribution of individual components. Several line shapes (Doniach-Šunjić,[42] Mahan,[43] and Voigt) were tested, and it was found that the symmetric Voigt functions (in combination with a Shirley-type[44] background) yielded the most convincing fits. The error in the binding energies is estimated from the precision with which the Fermi level could be determined (see Section S1). For pure Ag, the accuracy of the Fermi level was ±0.01 eV. The error bars increased with increasing Pd loading due to the proximity of the Pd 4d band to the Fermi level, leading to an increase of the estimated error to ±0.03 eV.

Scanning Tunneling Microscopy. The local structure of the PdAg alloy was investigated using a beetle-type scanner (RHK UHV VT STM) mounted inside a UHV chamber (base pressure $<1 \times 10^{-10}$ Torr). The preparation chamber was equipped with AES (retarding-field analyzer), LEED (OCI LPS075/300), and QMS (Balzers Prisma 80 QMS200) capabilities, an electron-beam evaporator (Focus EFM3T), and a sputter gun (Perkin Elmer 04-161). During Pd evaporation, the sample was water cooled. The sample temperature was measured with a K-type thermocouple clamped between the sample holder and the back of the sample.

The sample was imaged with cut PtIr tips, which were *in situ* conditioned by applying voltage pulses (0.5−3 V, both polarities, for 10−100 ms) while keeping the tip−sample separation fixed. Stronger conditioning was performed by moving the tip outside the region of interest and, first, increasing the voltage to 8−10 V and, second, increasing the current to 50 nA. After 1−3 h, the tunneling current was stepwise decreased. The images were recorded in a constant-current mode using a digital controller (RHK R9). The piezo scan tube was calibrated using monatomic steps on the Ag(111) surface and atomically resolved images of the Ag(111) surface, after drift correction. The images were corrected by subtracting a planar background.

Density Functional Theory Calculations. The alloy surface was modeled by using 6-layer slabs and either a (2×2) or (3×3) unit cell. The bottom 3 layers were fixed while the top 3 layers were fully optimized with a convergence threshold of 0.02 eV/Å. The oxidized surface was modeled by a supercell of 4 layers, with each of the bottom 3 layers consisting of 48 Ag atoms, while the top layer consists of 35 Pd atoms and 28 O atoms. The PBE functional[45] and a 450-eV-cutoff energy were used for all the calculations. $9 \times 9 \times 1$, $7 \times 7 \times 1$, and $3 \times 1 \times 1$ K-points were used for the (2×2) unit cell, (3×3) unit cell, and oxidized surface model, respectively. In the core-level-shift (CLS) calculations, the final-state approximation and half-electron excitation were used for all the species, except for the surface Pd bound by CO, for which one-electron excitation was used. Previous studies have shown that calculations with

final-state approximation and one-electron excitation reproduce accurately Pd 3d CLS in CO(ads)/Pd(111) compared to experiment.[46] Core-level shifts calculated with DFT have been shown to compare well to measured values, for example, the Pd 3d, C 1s, and O 1s CLS in CO(ads)/Pd(111);[46] the Rh 3d surface CLS of the bare Rh(111); and Rh 3d, C 1s, and O 1s shifts in CO(ads)/Rh(111).[47] Herein, the method was calibrated by calculating the surface core-level shift (SCLS) for Pd(111). The calculated SCLS is −0.18 eV, which is similar to the experimental value of −0.24 eV.[48] The difference was used as an estimate for the error bar on the calculated core-level shifts for PdAg alloys. All the calculations are performed with VASP.[49,50] A detailed description of the calculation methods is provided in the Supporting Information (Section S4).

RESULTS AND DISCUSSION

Structure of the Pd/Ag(111) Surface Alloy. Deposition of Pd (0.2 ML) at 290 K and annealing (405 K for 2 min) resulted in the formation of compact islands of tens of nanometers in size, 3 layers high with respect to the surrounding Ag(111) terrace (Figure 1a). This arrangement results in plateaus of 4 distinct heights (Figure 1b), including a layer lower than the original surface. The relative contributions were such that within this image 53% of the surface atoms were in the lowest level (−1), 9% of the surface atoms were one level higher (0), 10% were in the level above the original surface level (1), and finally, 28% of the surface atoms were in the layer two lattice parameters above the original surface (2).

The structure obtained after depositing Pd at room temperature is substantially different from that after annealing at 405 K (Figure S4, Section S5). Islands are also present at 300 K, but only 10−20% of them are multiple-layers high with adjacent vacancy islands and compact, like the annealed structure. Instead, most islands are only single-layer high and have a fractal shape after deposition at 290 K. These results suggest that a metastable structure is formed at room temperature.

Since the amount of deposited Pd (measured by AES, prior to annealing) was insufficient to form three-layer thick islands of pure Pd, the islands must contain a large amount of Ag. These three-layer-high islands can be formed by the incorporation of Ag atoms from the substrate into the islands, with Ag atoms forming a capping layer. This resulted in islands that were two-layers high with respect to the original surface plane (level 0), and three-layers high with respect to the etched surface layer (level −1). The driving force of this migration and the burying of Pd is the large difference in surface free energy between Pd and Ag, the former being 1.6 times higher.[34] The details regarding the energetics will be discussed below. The extent of substrate etching is rather large, as about half of the substrate atoms were removed, exposing the lower lying terrace (level −1). Since more Ag atoms (0.5 ML) were removed than required to cap all the islands at a Pd coverage of 0.2 ML, a significant amount of Ag must have been incorporated in the Pd-rich layer (level 1) below the Ag capping layer (level 2).

Only a small percentage of the surface atoms remained in the original terrace (level 0). Interestingly, these atoms are mostly located between the compact islands, interconnecting them. The atoms interconnecting the islands are in close vicinity of these islands and would be expected, kinetically, to be the first to migrate to the top of the islands to cover the Pd.

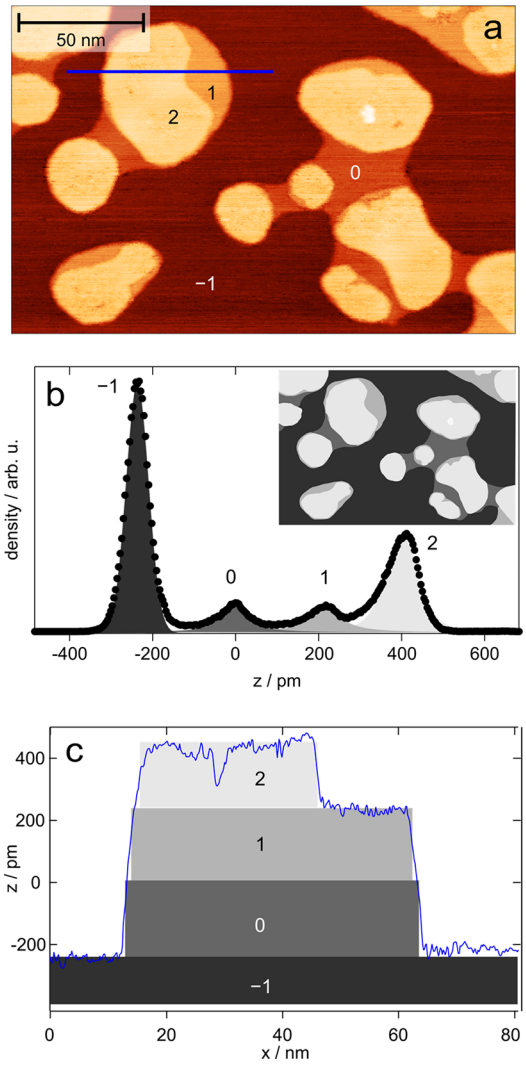

Figure 1. Multilayer islands form after deposition of Pd (0.2 ML) on Ag(111) at 290 K, followed by annealing to 405 K for 2 min. (a) STM image showing compact islands on a single Ag(111) terrace (see Figure S4, Section S5, Section S6 for full-size image). (b) The area distribution of plateaus of the four different heights on the surface with respect to the plane of the Ag(111) surface before deposition (level 0). Level −1 is due to substrate etching. Level 1 is a monolayer island height, and level 2 originates from a 3-layer island. The respective areas are 53% (−1), 9% (0), 10% (1), and 28% (2). STM details: U_{sample} = 30 mV, $I_{set\ point}$ = 1.0 nA. The relative areas are obtained directly from the STM scans and are thusly broadened by a tip size effect at the island boundaries. The frame shown is 199 nm × 129 nm. (c) Height profile along the blue line scan in part a depicting an island showing all layer heights. The gray and black boxes under the line scan illustrate the various heights in the island (colors match those of the height distribution).

However, this is clearly not the case, which hints that the Ag atoms in these positions are bonded more strongly.

A large fraction of the islands was covered by the capping layer, on the basis of the ratio of the number of surface atoms in level 2 to that in level 1 measured to be 2.8. However, it should be noted that a significant fraction of the island (level 1) was not capped (Figure 1c). To complete the capping, Ag atoms from either the interconnecting regions between the islands (level 0) or from level −1 would be required. Stabilization of the interconnecting Ag atoms (level 0)

quantitatively accounts for the deficit, and apparently the annealing temperature was too low to allow the migration of Ag atoms from layer −1. Notably, as the islands did not adsorb CO at temperatures sufficiently low to prevent rearrangement of this layered structure (117−130 K; see below), it is unlikely that any Pd is exposed in these layered structures. Thus, these observations suggest that Ag was both incorporated into level 1 and migrated on top of the island to form the capping layer (level 2). This structure is supported by both XPS and DFT calculations (see below). Similar structures formed on steps separating the flat Ag(111) terraces (Figure S6, Section S6).

Theoretical Models of Thermodynamic Stability of Pd/Ag(111). A Ag-capped PdAg alloy is thermodynamically the most favorable structure of the models considered using DFT for all concentrations of Pd (Figure 2 and Table 1), in agreement with the experimental data. Three different types of structures were explicitly considered for the alloys: (1) a Pd overlayer on top of Ag; (2) a surface alloy in which both Pd and Ag are in the top layer; and, (3) a Ag-capped Ag/Pd alloy layer on top of bulk Ag (Figure 2). Each of these structures was modeled as a function of Pd surface mole fraction in the range 0.25−1.00. Of these models, the capped alloy was always the most stable, followed by the surface alloy, with the Pd overlayer being the least stable (Figure 2). The stabilization of the subsurface alloy compared to the surface alloy was calculated to be ∼0.25 eV per Pd atom for all alloy compositions (Figure 2). This is in agreement with previously published calculations of the segregation energies for Pd atom in the top and second layers of Ag(111).[51,52]

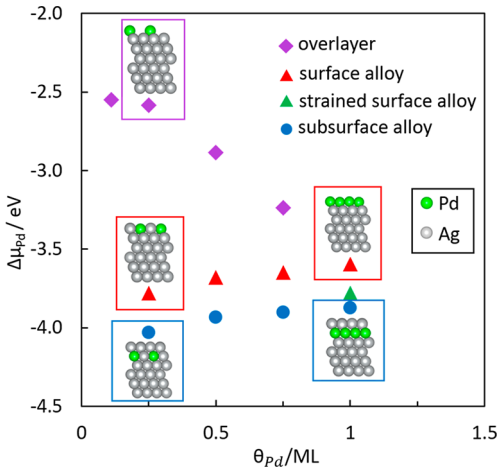

Figure 2. Computation of the change of Pd chemical potential indicates that the subsurface PdAg alloy is the most stable of the three different models considered for all Pd mole fractions. Pd is represented by green circles and Ag by the gray circles. Blue circles, subsurface Pd−Ag/Ag(111); red triangles, Pd surface alloy/Ag(111); purple diamonds, a Pd overlayer on Ag(111). The overlayer and surface structures converge for 1 ML of Pd. The overall stability decreases with increasing Pd coverage for both the surface and subsurface alloy, indicating that dispersion of Pd is slightly favored. Energies were calculated for 6-layer slabs in all cases using DFT (see Materials and Methods section). Diagrams show the side view of the surface.

The Pd chemical potential in the capped and surface alloys increases slightly (0.04 eV/Pd atom) with increasing Pd mole fraction, indicating some repulsion between Pd atoms, suggesting that Pd prefers to be surrounded by Ag in the alloy (Figure 2). In contrast, the chemical potential of the Pd in the overlayer decreases as the coverage increases. This change is attributed to the low coordination number of Pd at low mole fraction. As the Pd coverage increases, the average coordination of Pd also increases, reaching the limit of a full Pd layer at a mole fraction of 1.0 (Figure 2). Taken together, the Ag-capped alloy with Pd surrounded by Ag is the most stable model.

The effect of surface strain was estimated for a Pd mole fraction of 1, at which point the overlayer and the surface alloy are equivalent, yielding a surface terminated in Pd. Experimentally, it is possible that the top layer of Pd is not in registry with the Ag below but is somewhat compressed since the Pd and Ag lattice constants are slightly different in the bulk materials. Because the difference in lattice constants is small (∼5%), such a compression would occur over a very long length scale that is not currently tractable for DFT studies. Instead, it is simulated by using the (2 × 2) unit cell model for 1 ML Pd/Ag(111) with the lattice constant of the total system compressed to the value of the Pd(111) surface. The surface alloy is found to be stabilized (green triangle, Figure 2), but remains less stable than the Ag-capped alloy.

Photoelectron Spectroscopy of Ag/PdAg/Ag(111). The chemical environment of Pd deposited on Ag(111) and annealed to ∼400 K appears to be invariant with the Pd content over the range of coverages studied (0.06−0.27 ML), on the basis of the lack of variation of the Pd $3d_{5/2}$ binding energies and their peak widths measured using XPS (Figure 3). Specifically, the full width at half-maximum (fwhm) of the Pd $3d_{5/2}$ peak varied between 0.58 and 0.64 eV, and the peak position was between 334.87 ± 0.03 and 334.94 ± 0.02 eV. The Pd environment, therefore, appears to be similar for all Pd concentrations given the relatively small fwhm of the peaks and the fact that there was no correlation between both the width and the position and the Pd loading. Notably, there is a small shoulder in all Pd $3d_{5/2}$ spectra at higher binding energy (335.5−336 eV), which may be attributed to a small amount of Pd in the surface due to the presence of residual CO in the gas phase. The effect of CO is discussed in more detail below.

Table 1. Change in Pd Chemical Potential, $\Delta\mu_{Pd}$, and Core-Level Shift of the Pd Atoms in the Pd/Ag(111) Alloy

	$\Delta\mu_{Pd}$/eV			CLS/eV		
Pd coverage/ML	overlayer	surface	subsurface	overlayer	surface	subsurface
0.11	−2.55			−0.65		
0.25	−2.58	−3.78	−4.03	−0.66	−0.21	−0.06
0.50	−2.88	−3.68	−3.93	−0.61	−0.26	−0.12
0.75	−3.24	−3.65	−3.90	−0.45	−0.23	−0.08
1.00		−3.60	−3.87		−0.32	−0.14
1.00 (with strain)		−3.78			−0.15	

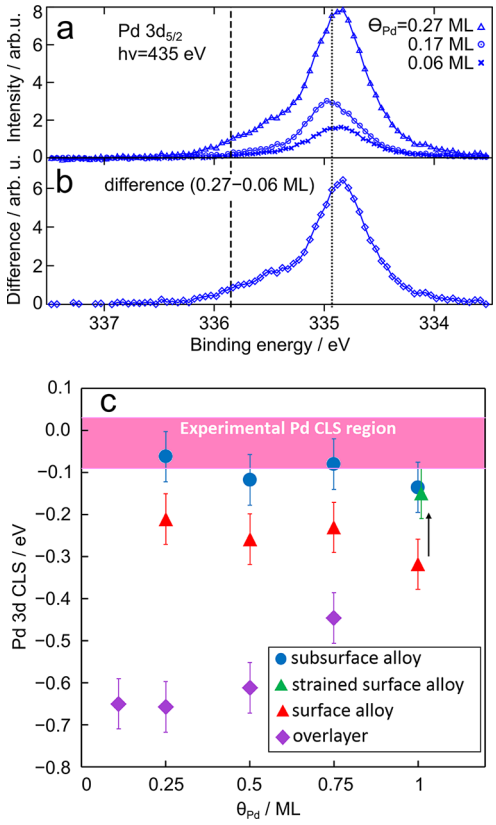

Figure 3. XPS and DFT provide evidence that Pd resides in the subsurface region after heating to 400 K. (a) Pd $3d_{5/2}$ spectra for various amounts of Pd deposited followed by heating to ~400 K show that the peak position is essentially independent of the Pd content and shifted negatively relative to the bulk Pd(111) peak at 334.93 eV (dotted line).[48] (b) Difference between the spectra for the highest Pd content (0.27 ML) and the lowest (0.06 ML), which demonstrates that there are no new features that arise due to increasing Pd exposure. The shoulder at higher binding energy in both parts a and b may be attributed to adsorption of background CO (Figure 5a). (c) Calculated Pd $3d_{5/2}$ core-level shifts (CLS) for the three different models considered: Pd in the subsurface (blue circles), in the surface (red triangles), and on top of the surface (purple diamonds). The calculated core-level shift for a strained Pd overlayer (1 ML Pd on top of Ag(111) with the lattice constant of Pd) is indicated by the green triangle. The CLS decreases from −0.36 to −0.15 eV after the lattice of the model was compressed to match the Pd lattice constant (green triangle). All spectra were recorded (beamline 9.3.2, ALS) with a photon energy of 435 eV, resulting in emission of photoelectrons with a kinetic energy of ~100 eV and an IMFP[53] of 0.4−0.5 nm.

The Pd $3d_{5/2}$ binding energy measured for the Pd/Ag(111) alloy of 334.9 eV indicates that the Pd resides below the surface after heating to 400 K. The binding energy of Pd $3d_{5/2}$ for bulk Pd(111) was previously measured to be 334.93 eV,[48] which is similar to that of the annealed Pd/Ag(111) alloy (Figure 3a). Furthermore, the core-level shift of Pd in the *surface* of bulk Pd is substantially more negative than that estimated for the Pd in the alloy on the basis of the XPS measurements. Specifically, the surface core-level shift (SCLS) for Pd(111) was measured to be −0.24 eV,[48] compared to a shift in the range −0.09 to 0.03 eV derived from the experimental measurements here (Figure 3a).

The calculated Pd 3d CLSs are also consistent with Pd residing in the subsurface layer (Figure 3c). The calculated Pd 3d CLS for subsurface Pd is −0.14 to −0.06 eV, in good agreement with the measured values of −0.09 to 0.03 eV. Furthermore, the calculated CLS for Pd in the subsurface alloy is essentially independent of the Pd concentration, also in agreement with the experimental results. The Pd 3d CLS varies between −0.06 eV for 0.25 ML of Pd to −0.14 eV for 1.0 ML of Pd. In contrast, the Pd 3d core-level shifts for Pd, either on top of the Ag(111) surface or in a surface alloy, are between −0.3 and −0.65 eV and between −0.2 and −0.3 eV, respectively, which are substantially larger and more negative than the experimental values. These differences are well outside the error of the calculations, estimated to be 0.06 eV (see Materials and Methods section). The numerical data is shown in Table 1.

Introduction of strain into the model for the surface alloy results in a CLS similar to the subsurface alloy for a Pd coverage of 1.0 ML (Figure 3c). (Note that, at 1.0 ML, the surface alloy and Pd overlayer are identical.) The CLS was simulated by calculating the core-level shift for a 1 ML Pd/Ag(111) structure with the lattice constant compressed to the value of the Pd(111) surface.

This model forces the compression to occur over an extremely short length scale and, therefore, will overestimate the effect. Within this model, the core-level shift for the Pd 3d peaks changes from −0.36 to −0.15 eV. While it is not possible to quantify the effect of strain in a realistic system, it is clear that strain will tend to decrease the core-level shifts.

The presence of a variety of chemical environments for the Ag in the alloy is indicated in surface-sensitive Ag $3d_{5/2}$ spectra of Pd/Ag(111) (Figure 4a, b), consistent with the conclusion that Ag caps the islands observed in STM (Figure 1) so as to create a distinct chemical environment (Figure 2). The Ag $3d_{5/2}$ peak is substantially broader for the alloy compared to that for pristine Ag(111) (Figure 4a). The fwhm of the Ag $3d_{5/2}$ peak increased from 0.51 eV for clean Ag(111) to 0.76 eV for the highest Pd loading (0.27 ML). The broadening was asymmetric and resulted in a concurrent shift from 368.14 ± 0.02 to 368.02 ± 0.03 eV. The difference between the spectra for pristine Ag(111) and that for the highest Pd coverage shows a strong intensity increase at 367.77 eV. These changes suggest that there are distinct core-level shifts for the Ag atoms below the islands (level 0), in the islands (level 1), and capping the islands (level 2). The difference spectrum shows that the average Ag core-level shift was around −0.4 eV, compared to Ag atoms in the surface or bulk of the pristine Ag(111) surface.

The shift to lower binding energy of the Ag $3d_{5/2}$ peak indicates that the average Pd−Ag coordination increases with higher Pd coverages, indicating that Ag disperses into the Pd (Figure 2). This conclusion is based on the linear correlation of the calculated Ag $3d_{5/2}$ CLS with the number of Pd neighbors (Figure 4c) and the corresponding shift to lower binding energy of the experimentally measured Ag $3d_{5/2}$ peak (Figure 4a,b). The shift stems from a higher fraction of Ag atoms coordinated to, possibly, more Pd with increasingly higher Pd coverages. The linear relationship is used to estimate the average number of Pd neighbors for Ag. For example, the average number of Pd neighbors for Ag is estimated to be 3 for 0.27 ML Pd on the basis of the Ag $3d_{5/2}$ shift of −0.2 eV for (Figure 4b,c).

The near-perfect linear correlation between the Ag 3d CLS and the number of Pd neighbors in structures having Ag atoms with various PdAg configurations shows that the exact PdAg configuration is not critical for the Ag 3d CLS. The linear scaling relationship between the Ag 3d surface CLS and the

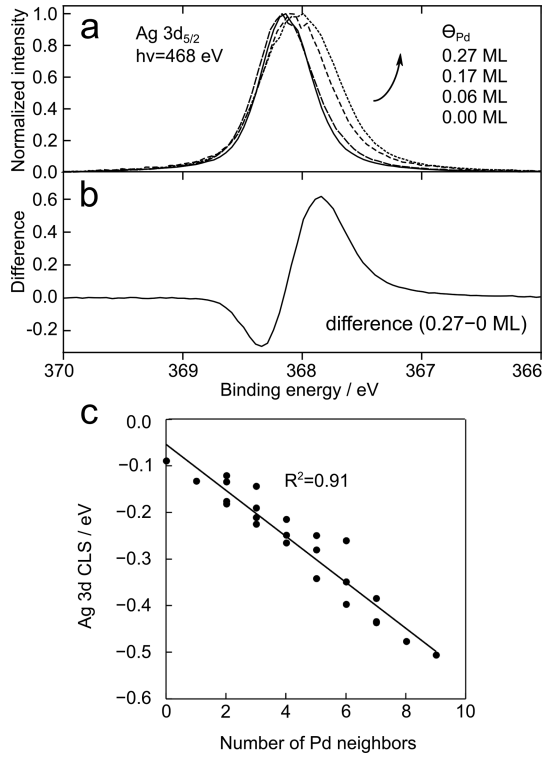

Figure 4. Shift to lower binding energy and broadening of the Ag 3d peaks as Pd content is increased indicate that Ag alloys with Pd, on the basis of (a) X-ray photoelectron data for the Ag $3d_{5/2}$ (a, b) and (c) calculation of the Ag 3d core-level shift (CLS) as a function of the number of Pd atom neighbors. The change in the Ag $3d_{5/2}$ peak is further illustrated in the difference spectrum (b) between pristine Ag(111) and Ag(111) with the highest Pd loading (0.22 ML). The experimental data were obtained after deposition of various amounts of Pd on Ag(111) at 300 K followed by annealing to 400 K. Surface-sensitive Ag $3d_{5/2}$ photoelectron spectra (a) were obtained using a photon energy of 468 eV, resulting in emission of photoelectrons with a kinetic energy of ∼100 eV and an IMFP[53] of 0.4−0.5 nm. The Ag $3d_{5/2}$ spectra were individually normalized to the maximum intensity to show the shape change of the Ag 3d peak irrespective of the intensity attenuation by Pd. Calculated Ag 3d core-level shifts (c) of various PdAg structures and pure Ag(111) without Pd neighbors, show that the CLS of surface Ag has a linear correlation with the number of Pd neighbors.

number of Pd neighbors was derived from calculation of the Ag 3d CLS for the Ag surface atoms (coordination number is 9) in a large array of surface and subsurface alloys (Figure S7 and Table S4, Section S7). The calculated CLS for surface Ag in pristine Ag(111) is −0.1 eV. The value is rather small, and it is not resolved in the experimental data.

The progressive broadening of the Ag 3d peaks with higher Pd coverage indicates that the variation in Ag−Pd coordination became higher with larger Pd coverage. This suggests that the in-plane mixing of Pd and Ag is slower for larger islands; therefore, these islands would exhibit a large concentration gradient form the perimeter to the center.

Exposure to CO. Exposure of the Ag/PdAg/Ag(111) surface alloy to CO (p_{CO} = 0.5 Torr) induces segregation of Pd to the surface even at room temperature, demonstrating the ability of the alloy to restructure even under moderate conditions. The resurfacing of Pd is important because at least a small amount of Pd needs to be at the surface for catalytic function.

The effect of CO exposure on the distribution of the Pd in the surface alloy was demonstrated using density functional theory and ambient-pressure XPS (Figure 5). At high

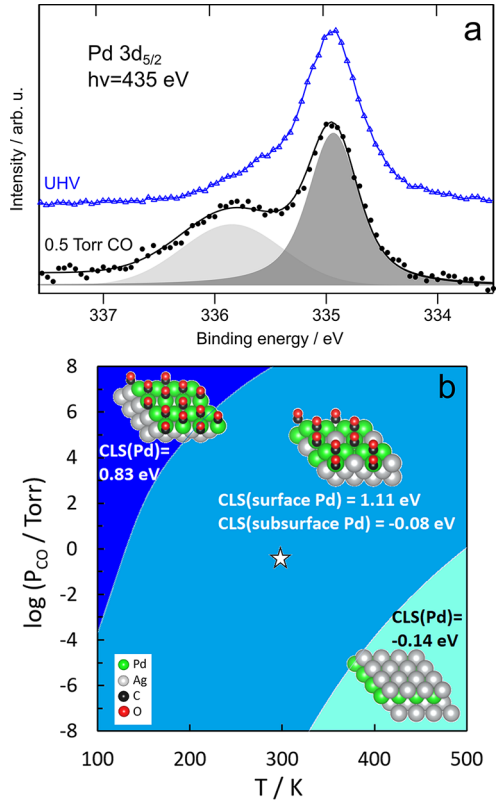

Figure 5. CO adsorption at room temperature leads to resurfacing of the Pd (0.27 ML). In the surface-sensitive Pd $3d_{5/2}$ photoelectron spectra (a), a new peak appears at 335.85 eV upon exposure to 0.5 Torr CO at room temperature (black curve). The main Pd $3d_{5/2}$ peak is also shifted to slightly higher binding energy relative to the peak for the as-prepared surface alloy under UHV conditions (blue curve). Spectra (a) were obtained using a photon energy of 435 eV, resulting in emission of photoelectrons with a kinetic energy of ∼100 eV and an IMFP[53] of 0.4−0.5 nm. DFT was used to generate a surface stability diagram of Pd/Ag(111) as a function of CO pressure and temperature (b). Pd, Ag, C, and O are colored green, gray, black, and red, respectively. At very low pressures and temperatures above 325 K, the most stable surface is pure Ag/Pd/Ag(111). At lower temperature and higher CO pressures, Pd segregation to the surface is favored. In the regime relevant to the experimental conditions (white star, middle region), 75% of the Pd is on the surface, bound to CO, with a CO to surface Pd ratio of 2:3. In the upper left region, all the Pd atoms in the subsurface are brought to the surface and are bound to CO, with a CO to surface Pd ratio of 3:4.

temperature and low pressure of CO, the subsurface Pd alloy is thermodynamically the most stable, as discussed above (lower right region in Figure 5b). For example, pure Ag/PdAg/Ag(111) is favored at 400 K and CO pressures below 10^{-4} Torr.

At higher CO pressure (0.5 Torr), resurfacing of Pd is shown by experimental measurements of a new peak in the Pd $3d_{5/2}$ spectrum associated with the presence of CO (Figure 5a). Density functional theory likewise predicts that the most stable phase is for Pd to reside on the surface, bound to CO, as the pressure increases and the temperature decreases (Figure 5b). Specifically, at 300 K and a pressure of 0.5 Torr (the

experimental conditions), 75% of the Pd atoms are on the surface and bound to CO. The CO preferentially adsorbs on the Pd_3 hollow sites, and the ratio of CO to the surface Pd is 2:3. At extremely high pressure and low temperature, the most stable structure is for all Pd to be on the surface, bound to CO (upper left corner of phase diagram, Figure 5b), with the ratio of CO to the surface Pd being 3:4. In this configuration, 2/3 of the CO are on the hollow sites and 1/3 of the CO are on the top sites. This adsorption pattern is the same as the adsorption of 0.75 ML CO on the Pd(111) surface.[54] The extreme conditions for which this structure becomes the most stable were experimentally not feasible.

Kinetic factors will also play a role in determining the actual surface coverage of Pd under various experimental conditions. Specifically, Pd must be sufficiently mobile to achieve the thermodynamic structure. Although CO is predicted to induce segregation of Pd to the surface below 275 K at CO pressures as low as 10^{-8} Torr (Figure 5b), no significant CO adsorption onto the annealed Pd/Ag(111) alloy is detected at 117−130 K (Figure S8, Section S8). This result is consistent with the conclusion that the islands formed (Figure 1) are capped by Ag. Even though resurfacing of Pd in the presence of CO is thermodynamically favored (Figure 5b), diffusion of Pd in Ag at these relatively low temperatures is expected to be significantly slower if the barrier were the same as for bulk diffusion (72−183 kJ/mol).[55] The estimated barrier based on the AP XPS measurements is ∼10 kJ/mol (0.1 eV) (see below).

For the structure on Figure 5b calculated to be the most stable under the experimental conditions (white star in Figure 5b) of the investigated structures (Figure S9, Table S5, Section S9), the surface Pd atoms bound to CO show a core-level shift of +1.11 eV, contrasting with the negative CLS calculated for Pd on the bare structure (Figure 3c). The Pd atom remaining in the subsurface keeps a CLS characteristic of such a subsurface position (−0.08 eV). The CLS for Pd bounded by CO is close to the experimental peak value (+0.91 eV). However, the peak is much broader than the peak of subsurface Pd (Figure 5a), and this is because the CLS is dependent on the Pd coverage in the model (considered as 1 ML in Figure 5b). Lower coverage values for Pd give higher CO/Pd ratios (up to 1) in the most favorable structure, providing Pd CLS values up to +1.62 eV, (see Figures S10 and S11 in Supporting Information). It is expected that various local amounts of Pd on the surface result in various CO-covered structures with a different CLS, which explains the broad Pd 3d peak. Altogether, these results convincingly demonstrate that the CO-induced resurfacing of Pd is thermodynamically feasible, and the amount of resurfaced Pd is dependent on the experimental conditions.

At 300 K, exposure of the Ag-covered islands to CO at a pressure of 0.5 Torr changed the Pd $3d_{5/2}$ spectrum drastically (Figure 5a), probed with AP XPS (beamline 9.3.2, ALS). The most notable change was the appearance of a new, rather broad peak at higher binding energy. Additionally, the main peak shifted slightly to higher binding energy. The spectrum was fitted to estimate the $3d_{5/2}$ binding energy of the two contributions, which were found at 335.85 ± 0.04 and 334.94 ± 0.02 eV, respectively. The latter was shifted with 0.07 eV with respect to the main Pd $3d_{5/2}$ peak, before CO exposure. The ratio of the two integrated peaks is 0.77 ($I_{334.94eV}/I_{335.85eV}$). Assuming that the peak at 334.94 eV originated from subsurface Pd and that it experienced an additional attenuation by the surface layer of $\exp\left(-\frac{d}{\lambda}\right)$, the attenuation-corrected intensity ratio becomes 1.28 (d was assumed to be equal to the monatomic step on Pd(111), 0.225 nm, and λ = 0.44 nm at KE = 100 eV[53]). This ratio hints that 4 out of 9 Pd atoms were present in the surface and binding CO directly.

The resurfacing of Pd at room temperature was relatively fast, indicative of a modest barrier, estimated to be at most 10 kJ/mol (0.1 eV). The spectral changes due to Pd resurfacing were observed in the first spectrum recorded approximately 1−2 min after increasing the CO pressure. The estimated barrier would lead to a residence time, $1/\exp(-E_a/RT)$, of Pd in subsurface layer of 55 s. Interestingly, this barrier is much lower than reported barriers for bulk diffusion in PdAg alloys of 72−183 kJ/mol (0.7−1.9 eV).[55]

The resurfacing of Pd associated with the adsorption CO is supported by the measured increase in Pd/Ag ratio upon CO exposure at room temperature. Before exposure of the sample, this ratio was 0.10, while it was 0.15 under the CO atmosphere. This increase originates both in the decreased shielding of the Pd by the CO adsorption layer compared to the Ag capping layer and the increased shielding of the Ag by the resurfaced Pd and the CO(ads).

Oxidation of Ag/Pd/Ag(111). Clear evidence of Pd oxidation and migration of Pd to the surface was obtained using XPS following exposure of the Ag/PdAg/Ag(111) surface alloy to O_2 (1.0 Torr) at 400 K (Figure 6a). The appearance of a broad shoulder in the Pd $3d_{5/2}$ spectrum at higher binding energy (335.5−337 eV) is a clear sign of oxidation. Several different oxide structures (surface oxide, PdO clusters on the surface oxide, and bulk PdO) have been attributed to Pd $3d_{5/2}$ binding energies between 335.5 and 336.6 eV.[56] The fact that the O-induced peak was very broad and without a clear maximum suggests the presence of multiple oxide species and an incomplete oxidation of the Pd.

Metallic Pd is still present in the alloy after oxidation at 400 K in 1 Torr O_2, on the basis of the persistence of the Pd $3d_{5/2}$ peak at 335.0 eV (Figure 6a). Although repeated oxidation at 400 K decreased the intensity of the metallic Pd peak and concurrently increased the intensity of the shoulder at higher binding energy, complete oxidation of the Pd was not achieved. In fact, the incremental changes in the spectrum lessened with each exposure, indicating that the rate of oxidation decreased after the initial oxidation step.

The inability to fully oxidize all Pd could be explained by either kinetic effects that prevent Pd migration to the external surface where it can be oxidized or, thermodynamically, stabilization of an interfacial layer of metallic Pd between the oxidized Pd and the Ag. Oxidation at higher temperature to test the possibility of kinetic limitations was not experimentally feasible because annealing results in the dissolution of Pd into the bulk of Ag.

A model of the Pd oxide was created using DFT, on the basis of the known structures of 2-dimensional surface oxides on Pd. Oxidation of Pd(111) yields a 2-D Pd_5O_4 compound, having a $(\sqrt{6}\times\sqrt{6})$ unit cell and a thickness of one layer,[57−60] and theoretical studies show that Pd_5O_4 is the most thermodynamically stable surface oxide on Pd(111).[61] Since the Ag lattice is only 5% larger than Pd, the model adopted for the alloy is a 2-D Pd oxide on top of Ag(111) (Figure 6b). Using this model (Figure 6b), the stability of the Pd_5O_4 overlayer vs the Pd alloy was investigated as a function of O_2

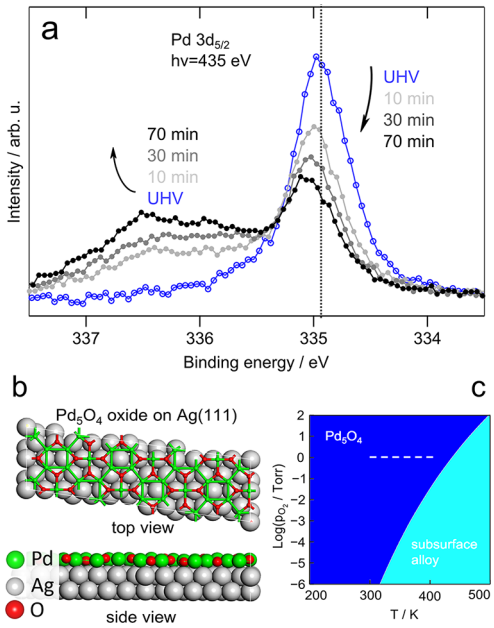

Figure 6. Exposure of the Ag/PdAg/Ag(111) alloy (0.17 ML) to O_2 at 400 K induces migration of Pd to the surface and formation of a Pd oxide layer. (a) Surface-sensitive Pd $3d_{5/2}$ photoelectron spectra show the development of a broad shoulder at higher binding energy assigned to oxidized Pd. (The spectrum of the as-prepared alloy is in blue and the alloy exposed to O_2 in gray and black.) Dotted line indicates position of bulk Pd.[48] Spectra were recorded after (1) cooling to room temperature and (2) evacuation of the O_2 atmosphere. Surface-sensitive Pd $3d_{5/2}$ photoelectron spectra (a) were obtained using a photon energy of 435 eV, resulting in emission of photoelectrons with a kinetic energy of ~100 eV and an IMFP[53] of 0.4−0.5 nm. (b) Oxidation of the Pd is predicted on the basis of the surface stability diagram of Pd/Ag(111) in O_2. The dashed line represents the experimental pressure and temperature range. (c) The Pd_5O_4/Ag(111) surface oxide is predicted to be stable at high O_2 pressures and/or lower temperature, using DFT. On the basis of the stability diagram (b), the surface oxide will persist at lower temperature even under vacuum conditions once formed at higher T and p.

pressure and temperature (Figure 6c). The change in chemical potential ($\Delta\mu_{Pd}$) was calculated by using the same unit cell to reduce the errors in the model. At an O_2 pressure of 1 Torr, the surface oxide is predicted to be the thermodynamically stable phase up to a temperature of 435 K (Figure 6c), which agrees with the measurements. The proposed model should only be considered as a simplified model for the oxidation process as Ag could also be oxidized to form mixed metal oxides. This model surface oxide Pd_5O_4 already shows a higher stability than Pd subsurface alloy under experimental conditions, which demonstrates the possibility of inverse segregation of Pd under even modest oxygen pressure.

SUMMARIZING DISCUSSION

Our studies led us to propose a model of Pd/Ag(111) demonstrating several key features that are important to understand catalysis driven by PdAg alloys (Figure 7). First, a clean and reduced surface of a PdAg alloy will generally be terminated by Ag, on the basis of a combination of STM, XPS, and DFT. Hence, there will be little if any Pd available for reaction on the surface in a dilute alloy, *if* it were devoid of other adsorbates. Furthermore, Pd is more stable when

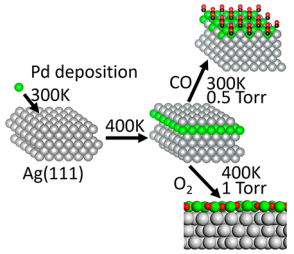

Figure 7. Schematic representation summarizing this work. A clean and reduced surface of Ag-terminated PdAg alloy forms at 400 K under vacuum. Palladium can be drawn to the surface by exposure to reactant gases, CO and O_2.

dispersed in Ag in a clean alloy, so that Pd tends to be surrounded by Ag, i.e., mainly in the form of single atoms.

Palladium can be drawn to the surface by exposure to reactant gases, CO and O_2, which has important implications for catalyst activation and sustained function. Hence, these reactive gases can be used in catalyst pretreatments to enrich the surface of a catalyst in Pd to increase reactivity.

The driving force for Pd enrichment in the surface is the creation of a stronger Pd−CO bond relative to the Ag−CO bond. By drawing Pd to the surface, the Pd is potentially available for reaction with, for example, alkynes. The Pd-rich surface is predicted to persist even at low pressures of CO (10^{-6} Torr) and temperatures below 300 K (Figure 5). CO could also inhibit other reactions because of its strong bonding to the Pd sites. A similar phenomenon has been reported previously for $Rh_{0.5}Pd_{0.5}$ nanoparticles in that exposure to CO [p = 0.1 Torr; T = 300 °C (573 K)] induced segregation of Pd to the surface.[3] In this prior work, the temperature was sufficiently high to ease diffusion of metals in the bimetallic nanoparticle.

Kinetics are also important in determining surface composition. Segregation of Pd to the surface in the Ag/PdAg/Ag(111) alloy induced by CO (p = 0.5 Torr) is experimentally observed at room temperature but not at low temperatures (below 130 K). On the basis of these experiments, the mobility of Pd in PdAg alloys should be sufficient under catalytic conditions for compositional changes to be driven toward the thermodynamically favorable state in which Pd is enriched on the surface.

The enrichment driven by CO at room temperature also has important implications for the use of the CO stretch frequency, measured by diffuse-reflectance infrared Fourier-transform spectroscopy (DRIFTS). Typically, DRIFTS is performed by flowing CO over catalyst material at room temperature for an extended period. Indeed, Pd_xAg_{1-x} (x = 0.20−1.0) nanoparticles used CO DRIFTS to conclude that Pd and Ag are mixed and that Pd is on the surface.[62] These Pd_xAg_{1-x} nanoparticles were active for CO oxidation, consistent with the expectation that both CO and oxygen draw Pd to the surface. On the other hand, different pretreatments and other reactions may not result in the same surface composition, questioning the use of CO DRIFTS for evaluating the distribution and composition of alloy surfaces under reaction conditions.

Our work also suggests that pretreatment of PdAg catalysts by treatment with O_2, as used for the Pd_xAg_{1-x} nanoparticles[62] described above, will induce segregation of Pd to the surface in the form of a surface oxide. Once the Pd is on the surface, it can participate in reactions, such as CO oxidation. Calcining

(treatment with oxygen while heating) is a common pretreatment in heterogeneous catalysis. The work described herein suggests that treatment with oxygen induces fundamental changes in catalyst composition that could significantly affect catalytic function.

CONCLUSIONS

A strong dependence of the surface composition of AgPd alloys on the presence of ambient gases and temperature was demonstrated using a combination of STM, AP-XPS, and DFT. A model system was created by depositing Pd onto Ag(111), in which the most stable form of the reduced, clean alloy is a PdAg alloy capped by Ag on top of Ag(111). The presence of CO or reaction with O_2 favors enrichment of the surface in Pd. The strong bonding of CO to Pd relative to Ag induces surface segregation of Pd even for CO pressures as low as 10^{-6} Torr, on the basis of DFT models. Experimentally, Pd segregation is observed at room temperature but not at low temperature (<130 K). This difference is attributed to the slow diffusion of Pd at lower temperatures. Exposure to O_2 (300–400 K) leads to the formation of a Pd oxide surface layer. These results contribute significantly to the design of pretreatment processes for PdAg alloy catalysts and also for using CO DRIFTS to evaluate the state of the catalyst surface during reaction conditions.

ASSOCIATED CONTENT

Supporting Information

The Supporting Information is available free of charge on the ACS Publications website at DOI: 10.1021/acs.jpcc.8b08849.

Additional experimental and computational details; characterization of the clean Ag(111) surface using LEED, ISS, and AES; details regarding Pd quantification using XPS and AES; UHV XPS showing the absence of CO(ads) at 117–130 K on the annealed Pd/Ag(111) alloys; structures and CLS of various Pd/Ag(111) alloys; and coordinates of Pd_5O_4/Ag(111) (PDF)

AUTHOR INFORMATION

Corresponding Author

*E-mail: friend@fas.harvard.edu.

ORCID

Tobias Egle: 0000-0003-1670-9754

Miquel B. Salmeron: 0000-0002-2887-8128

Philippe Sautet: 0000-0002-8444-3348

Cynthia M. Friend: 0000-0002-8673-9046

Author Contributions

◆M.A.v.S. and K.D. contributed equally.

Notes

The authors declare no competing financial interest.

ACKNOWLEDGMENTS

The staff of beamline 9.3.2, especially Slavomir Nemsak, is gratefully acknowledged for its support. This research used resources of the Advanced Light Source, which is a DOE Office of Science User Facility under Contract DE-AC02-05CH11231. This work was supported as part of the Integrated Mesoscale Architectures for Sustainable Catalysis, an Energy Frontier Research Center funded by the U.S. Department of Energy, Office of Science, Basic Energy Sciences, under Award DE-SC0012573. The DFT calculations were performed on the HOFFMAN2 cluster at the UCLA Institute for Digital Research and Education (IDRE), and computing resources at Extreme Science and Engineering Discovery Environment (XSEDE) through the allocation CHE170060. XSEDE is supported by National Science Foundation Grant ACI-1548562.[63]

REFERENCES

(1) Alayoglu, S.; Beaumont, S. K.; Zheng, F.; Pushkarev, V. V.; Zheng, H.; Iablokov, V.; Liu, Z.; Guo, J.; Kruse, N.; Somorjai, G. A. CO_2 Hydrogenation Studies on Co and CoPt Bimetallic Nanoparticles Under Reaction Conditions Using TEM, XPS and NEXAFS. *Top. Catal.* **2011**, *54*, 778–785.

(2) Xin, H. L.; Alayoglu, S.; Tao, R.; Genc, A.; Wang, C.-M.; Kovarik, L.; Stach, E. A.; Wang, L.-W.; Salmeron, M.; Somorjai, G. A.; et al. Revealing the Atomic Restructuring of Pt–Co Nanoparticles. *Nano Lett.* **2014**, *14*, 3203–3207.

(3) Tao, F.; Grass, M. E.; Zhang, Y.; Butcher, D. R.; Renzas, J. R.; Liu, Z.; Chung, J. Y.; Mun, B. S.; Salmeron, M.; Somorjai, G. A. Reaction-Driven Restructuring of Rh-Pd and Pt-Pd Core-Shell Nanoparticles. *Science* **2008**, *322*, 932–934.

(4) Michalak, W. D.; Krier, J. M.; Alayoglu, S.; Shin, J.-Y.; An, K.; Komvopoulos, K.; Liu, Z.; Somorjai, G. A. CO Oxidation on PtSn Nanoparticle Catalysts Occurs at the Interface of Pt and Sn Oxide Domains Formed under Reaction Conditions. *J. Catal.* **2014**, *312*, 17–25.

(5) Menning, C. A.; Hwu, H. H.; Chen, J. G. Experimental and Theoretical Investigation of the Stability of Pt-3d-Pt(111) Bimetallic Surfaces under Oxygen Environment. *J. Phys. Chem. B* **2006**, *110*, 15471–15477.

(6) Zugic, B.; Wang, L.; Heine, C.; Zakharov, D. N.; Lechner, B. A. J.; Stach, E. A.; Biener, J.; Salmeron, M.; Madix, R. J.; Friend, C. M. Dynamic Restructuring Drives Catalytic Activity on Nanoporous Gold–Silver Alloy Catalysts. *Nat. Mater.* **2017**, *16*, 558–564.

(7) Zhang, Q.; Li, J.; Liu, X.; Zhu, Q. Synergetic Effect of Pd and Ag Dispersed on Al_2O_3 in the Selective Hydrogenation of Acetylene. *Appl. Catal., A* **2000**, *197*, 221–228.

(8) Pachulski, A.; Schödel, R.; Claus, P. Performance and Regeneration Studies of Pd–Ag/Al_2O_3 Catalysts for the Selective Hydrogenation of Acetylene. *Appl. Catal., A* **2011**, *400*, 14–24.

(9) Takht Ravanchi, M.; Sahebdelfar, S. Pd-Ag/Al_2O_3 Catalyst: Stages of Deactivation in Tail-End Acetylene Selective Hydrogenation. *Appl. Catal., A* **2016**, *525*, 197–203.

(10) Lamb, R. N.; Ngamsom, B.; Trimm, D. L.; Gong, B.; Silveston, P. L.; Praserthdam, P. Surface Characterisation of Pd–Ag/Al_2O_3 Catalysts for Acetylene Hydrogenation Using an Improved XPS Procedure. *Appl. Catal., A* **2004**, *268*, 43–50.

(11) Pei, G. X.; Liu, X. Y.; Wang, A.; Lee, A. F.; Isaacs, M. A.; Li, L.; Pan, X.; Yang, X.; Wang, X.; Tai, Z.; et al. Ag Alloyed Pd Single-Atom Catalysts for Efficient Selective Hydrogenation of Acetylene to Ethylene in Excess Ethylene. *ACS Catal.* **2015**, *5*, 3717–3725.

(12) Aich, P.; Wei, H.; Basan, B.; Kropf, A. J.; Schweitzer, N. M.; Marshall, C. L.; Miller, J. T.; Meyer, R. Single-Atom Alloy Pd–Ag Catalyst for Selective Hydrogenation of Acrolein. *J. Phys. Chem. C* **2015**, *119*, 18140–18148.

(13) Backx, C.; de Groot, C. P. M.; Biloen, P. Electron Energy Loss Spectroscopy and Its Applications. *Appl. Surf. Sci.* **1980**, *6*, 256–272.

(14) Barteau, M. A.; Madix, R. J. Low-Pressure Oxidation Mechanism and Reactivity of Propylene on Silver(110) and Relation to Gas-Phase Acidity. *J. Am. Chem. Soc.* **1983**, *105*, 344–349.

(15) Ayre, C. R.; Madix, R. J. π, π-Allyl, and Trimethylenemethane Complexes Derived from Isobutylene Adsorption on Oxygen-Activated Ag(110). *Surf. Sci.* **1992**, *262* (1–2), 51–67.

(16) Williams, F. J.; Bird, D. P. C.; Sykes, E. C. H.; Santra, A. K.; Lambert, R. M. Molecular Conformation of Styrene on Ag(100): Relevance to an Understanding of the Catalytic Epoxidation of Terminal Alkenes. *J. Phys. Chem. B* **2003**, *107*, 3824–3828.

(17) Klust, A.; Madix, R. J. Partial Oxidation of Higher Olefins on Ag(1 1 1): Conversion of Styrene to Styrene Oxide, Benzene, and Benzoic Acid. *Surf. Sci.* **2006**, *600*, 5025−5040.
(18) Barteau, M. A.; Madix, R. J. Acetylenic Complex Formation and Displacement via Acid-Base Reactions on Ag(110). *Surf. Sci.* **1982**, *115*, 355−381.
(19) Stuve, E. M.; Madix, R. J.; Sexton, B. A. Characterization of the Adsorption and Reaction of Acetylene on Clean and Oxygen Covered Ag(110) by EELS. *Surf. Sci.* **1982**, *123*, 491−504.
(20) Barteau, M. A.; Bowker, M.; Madix, R. J. Acid-Base Reactions on Solid Surfaces: The Reactions of HCOOH, H_2CO, and $HCOOCH_3$ with Oxygen on Ag(110). *Surf. Sci.* **1980**, *94*, 303−322.
(21) Zhou, L.; Madix, R. J. Oxidation of Styrene and Phenylacetaldehyde on Ag(111): Evidence for Transformation of Surface Oxametallacycle. *J. Phys. Chem. C* **2008**, *112*, 4725−4734.
(22) Wachs, I. E.; Madix, R. J. The Oxidation of Methanol on a Silver (110) Catalyst. *Surf. Sci.* **1978**, *76*, 531−558.
(23) Brainard, R. L.; Madix, R. J. Oxidation of Tert-Butyl Alcohol to Isobutylene Oxide: Rate-Limiting Carbon-Hydrogen Activation by a Ag(110) Surface. *J. Am. Chem. Soc.* **1987**, *109*, 8082−8083.
(24) Ayre, C. R.; Madix, R. J. The Adsorption and Reaction of 1,2-Propanediol on Ag(110) under Oxygen Lean Conditions. *Surf. Sci.* **1994**, *303*, 279−296.
(25) Sprunger, P. T.; Plummer, E. W. Interaction of Hydrogen with the Ag(110) Surface. *Phys. Rev. B: Condens. Matter Mater. Phys.* **1993**, *48*, 14436−14446.
(26) Zhou, X.-L.; White, J. M.; Koel, B. E. Chemisorption of Atomic Hydrogen on Clean and Cl-Covered Ag(111). *Surf. Sci.* **1989**, *218*, 201−210.
(27) Lee, G.; Sprunger, P. T.; Okada, M.; Poker, D. B.; Zehner, D. M.; Plummer, E. W. Chemisorption of Hydrogen on the Ag(111) Surface. *J. Vac. Sci. Technol., A* **1994**, *12*, 2119−2123.
(28) Bron, M.; Teschner, D.; Knop-Gericke, A.; Jentoft, F. C.; Kröhnert, J.; Hohmeyer, J.; Volckmar, C.; Steinhauer, B.; Schlögl, R.; Claus, P. Silver as Acrolein Hydrogenation Catalyst: Intricate Effects of Catalyst Nature and Reactant Partial Pressures. *Phys. Chem. Chem. Phys.* **2007**, *9*, 3559−3569.
(29) Brandt, K.; Chiu, M. E.; Watson, D. J.; Tikhov, M. S.; Lambert, R. M. Chemoselective Catalytic Hydrogenation of Acrolein on Ag(111): Effect of Molecular Orientation on Reaction Selectivity. *J. Am. Chem. Soc.* **2009**, *131*, 17286−17290.
(30) Brandt, K.; Chiu, M. E.; Watson, D. J.; Tikhov, M. S.; Lambert, R. M. Adsorption Geometry Determines Catalytic Selectivity in Highly Chemoselective Hydrogenation of Crotonaldehyde on Ag(111). *J. Phys. Chem. C* **2012**, *116*, 4605−4611.
(31) Liu, W.; Jiang, Y.; Dostert, K. H.; O'Brien, C. P.; Riedel, W.; Savara, A.; Schauermann, S.; Tkatchenko, A. Catalysis beyond Frontier Molecular Orbitals: Selectivity in Partial Hydrogenation of Multi-Unsaturated Hydrocarbons on Metal Catalysts. *Sci. Adv.* **2017**, *3*, e1700939.
(32) Liu, X.; Madix, R. J.; Friend, C. M. Unraveling Molecular Transformations on Surfaces: A Critical Comparison of Oxidation Reactions on Coinage Metals. *Chem. Soc. Rev.* **2008**, *37*, 2243−2261.
(33) Mäki-Arvela, P.; Hájek, J.; Salmi, T.; Murzin, D. Y. Chemoselective Hydrogenation of Carbonyl Compounds over Heterogeneous Catalysts. *Appl. Catal., A* **2005**, *292*, 1−49.
(34) Skriver, H. L.; Rosengaard, N. M. Surface Energy and Work Function of Elemental Metals. *Phys. Rev. B: Condens. Matter Mater. Phys.* **1992**, *46*, 7157−7168.
(35) Wouda, P. T.; Schmid, M.; Nieuwenhuys, B. E.; Varga, P. STM Study of the (111) and (100) Surfaces of PdAg. *Surf. Sci.* **1998**, *417*, 292−300.
(36) Wouda, P. T.; Schmid, M.; Nieuwenhuys, B. E.; Varga, P. Adsorbate Migration on PdAg(111). *Surf. Sci.* **1999**, *423*, L229−L235.
(37) Walle, L. E.; Grönbeck, H.; Fernandes, V. R.; Blomberg, S.; Farstad, M. H.; Schulte, K.; Gustafson, J.; Andersen, J. N.; Lundgren, E.; Borg, A. Surface Composition of Clean and Oxidized Pd $_{75}Ag_{25}$(100) from Photoelectron Spectroscopy and Density Functional Theory Calculations. *Surf. Sci.* **2012**, *606*, 1777−1782.
(38) Vignola, E.; Steinmann, S. N.; Vandegehuchte, B. D.; Curulla, D.; Sautet, P. C_2H_2-Induced Surface Restructuring of Pd−Ag Catalysts: Insights from Theoretical Modeling. *J. Phys. Chem. C* **2016**, *120*, 26320.
(39) Vignola, E.; Steinmann, S. N.; Le Mapihan, K.; Vandegehuchte, B. D.; Curulla, D.; Sautet, P. Acetylene Adsorption on Pd−Ag Alloys: Evidence for Limited Island Formation and Strong Reverse Segregation from Monte Carlo Simulations. *J. Phys. Chem. C* **2018**, *122*, 15456−15463.
(40) Seah, M. P.; Gilmore, I. S.; Beamson, G. XPS: Binding Energy Calibration of Electron Spectrometers 5—Re-Evaluation of the Reference Energies. *Surf. Interface Anal.* **1998**, *26*, 642−649.
(41) Krause, M. O.; Ferreira, J. G. K X-Ray Emission Spectra of Mg and Al. *J. Phys. B: At. Mol. Phys.* **1975**, *8*, 2007−2014.
(42) Doniach, S.; Šunjić, M. Many-Electron Singularity in X-Ray Photoemission and X-Ray Line Spectra from Metals. *J. Phys. C: Solid State Phys.* **1970**, *3*, 285−291.
(43) Mahan, G. D. Collective Excitations in X-Ray Spectra of Metals. *Phys. Rev. B* **1975**, *11*, 4814−4824.
(44) Shirley, D. A. High-Resolution X-Ray Photoemission Spectrum of the Valence Bands of Gold. *Phys. Rev. B* **1972**, *5*, 4709−4714.
(45) Perdew, J. P.; Burke, K.; Ernzerhof, M. Generalized Gradient Approximation Made Simple. *Phys. Rev. Lett.* **1996**, *77*, 3865−3868.
(46) Martin, N. M.; Van den Bossche, M.; Grönbeck, H.; Hakanoglu, C.; Zhang, F.; Li, T.; Gustafson, J.; Weaver, J. F.; Lundgren, E. CO Adsorption on Clean and Oxidized Pd(111). *J. Phys. Chem. C* **2014**, *118*, 1118−1128.
(47) Birgersson, M.; Almbladh, C.-O.; Borg, M.; Andersen, J. N. Density-Functional Theory Applied to Rh(111) and CO/Rh(111) Systems: Geometries, Energies, and Chemical Shifts. *Phys. Rev. B: Condens. Matter Mater. Phys.* **2003**, *67*, 045402.
(48) Andersen, J. N.; Hennig, D.; Lundgren, E.; Methfessel, M.; Nyholm, R.; Scheffler, M. Surface Core-Level Shifts of Some 4d-Metal Single-Crystal Surfaces: Experiments and Ab Initio Calculations. *Phys. Rev. B: Condens. Matter Mater. Phys.* **1994**, *50*, 17525−17533.
(49) Kresse, G.; Hafner, J. Ab Initio Molecular-Dynamics Simulation of the Liquid-Metal−Amorphous-Semiconductor Transition in Germanium. *Phys. Rev. B: Condens. Matter Mater. Phys.* **1994**, *49*, 14251−14269.
(50) Kresse, G.; Hafner, J. Ab Initio Molecular Dynamics for Liquid Metals. *Phys. Rev. B: Condens. Matter Mater. Phys.* **1993**, *47*, 558−561.
(51) Christensen, A.; Ruban, A.; Stoltze, P.; Jacobsen, K.; Skriver, H.; Nørskov, J.; Besenbacher, F. Phase Diagrams for Surface Alloys. *Phys. Rev. B: Condens. Matter Mater. Phys.* **1997**, *56*, 5822−5834.
(52) Hammer, B.; Nørskov, J. K. Theoretical Surface Science and Catalysis—Calculations and Concepts. *Adv. Catal.* **2000**, *45*, 71−129.
(53) Shinotsuka, H.; Tanuma, S.; Powell, C. J.; Penn, D. R. Calculations of Electron Inelastic Mean Free Paths. X. Data for 41 Elemental Solids over the 50 eV to 200 keV Range with the Relativistic Full Penn Algorithm. *Surf. Interface Anal.* **2015**, *47*, 871−888.
(54) Loffreda, D.; Simon, D.; Sautet, P. Dependence of Stretching Frequency on Surface Coverage and Adsorbate-Adsorbate Interactions: A Density-Functional Theory Approach of CO on Pd(111). *Surf. Sci.* **1999**, *425*, 68−80.
(55) Shu, J.; Adnot, A.; Grandjean, B. P. A.; Kaliaguine, S. Structurally Stable Composite Pd-Ag Alloy Membranes: Introduction of a Diffusion Barrier. *Thin Solid Films* **1996**, *286*, 72−79.
(56) Ketteler, G.; Ogletree, D. F.; Bluhm, H.; Liu, H.; Hebenstreit, E. L. D.; Salmeron, M. In Situ Spectroscopic Study of the Oxidation and Reduction of Pd(111). *J. Am. Chem. Soc.* **2005**, *127*, 18269−18273.
(57) Van Spronsen, M. A.; Frenken, J. W. M.; Groot, I. M. N. Surface Science under Reaction Conditions: CO Oxidation on Pt and Pd Model Catalysts. *Chem. Soc. Rev.* **2017**, *46*, 4347−4374.
(58) Lundgren, E.; Kresse, G.; Klein, C.; Borg, M.; Andersen, J. N.; De Santis, M.; Gauthier, Y.; Konvicka, C.; Schmid, M.; Varga, P. Two-Dimensional Oxide on Pd(111). *Phys. Rev. Lett.* **2002**, *88*, 246103.

(59) Zemlyanov, D.; Aszalos-Kiss, B.; Kleimenov, E.; Teschner, D.; Zafeiratos, S.; Hävecker, M.; Knop-Gericke, A.; Schlögl, R.; Gabasch, H.; Unterberger, W.; et al. In Situ XPS Study of Pd(1 1 1) Oxidation. Part 1:2D Oxide Formation in 10^{-3} mbar O_2. *Surf. Sci.* **2006**, *600*, 983−994.
(60) Duan, Z.; Henkelman, G. CO Oxidation on the Pd(111) Surface. *ACS Catal.* **2014**, *4*, 3435−3443.
(61) Klikovits, J.; Napetschnig, E.; Schmid, M.; Seriani, N.; Dubay, O.; Kresse, G.; Varga, P. Surface Oxides on Pd(111): STM and Density Functional Calculations. *Phys. Rev. B: Condens. Matter Mater. Phys.* **2007**, *76*, 045405.
(62) Ström, L.; Ström, H.; Carlsson, P.-A.; Skoglundh, M.; Härelind, H. Catalytically Active Pd−Ag Alloy Nanoparticles Synthesized in Microemulsion Template. *Langmuir* **2018**, *34*, 9754−9761.
(63) Towns, J.; Cockerill, T.; Dahan, M.; Foster, I.; Gaither, K.; Grimshaw, A.; Hazlewood, V.; Lathrop, S.; Lifka, D.; Peterson, G. D.; et al. XSEDE: Accelerating Scientific Discovery. *Comput. Sci. Eng.* **2014**, *16*, 62−74.